Modeling of Welded Joints in a Pyramidal Truss Sandwich Panel Using Beam and Shell Finite Elements

Ke Yuan
Department of Mechanical Engineering,
University of Maryland,
Baltimore County,
1000 Hilltop Circle,
Baltimore, MD 21250
e-mail: kyuan1@umbc.edu

Weidong Zhu[1]
Department of Mechanical Engineering,
University of Maryland,
Baltimore County,
1000 Hilltop Circle,
Baltimore, MD 21250
e-mail: wzhu@umbc.edu

Pyramidal truss sandwich panels (PTSPs) are widely used in engineering structures and their face sheets and core parts are generally bonded by the welding process. A large number of solid elements are usually required in the finite element (FE) model of a PTSP with welded joints to obtain its accurate modal parameters. Ignoring welded joints of the PTSP can save many degrees of freedom (DOFs), but significantly change its natural frequencies. This study aims to accurately determine modal parameters of a PTSP with welded joints with much fewer DOFs than those of its solid element model and to obtain its operational modal analysis results by avoiding missing its modes. Two novel methods that consider welded joints as equivalent stiffness are proposed to create beam-shell element models of the PTSP. The main step is to match stiffnesses of beam and shell elements of a welded joint with those of its solid elements. Compared with the solid element model of the PTSP, its proposed models provide almost the same levels of accuracy for natural frequencies and mode shapes for the first 20 elastic modes, while reducing DOFs by about 98% for the whole structure and 99% for each welded joint. The first 14 elastic modes of a PTSP specimen that were measured without missing any modes by synchronously capturing its two-faced vibrations through use of a three-dimensional scanning laser vibrometer (SLV) and a mirror experimentally validate its beam-shell element models created by the two proposed methods. [DOI: 10.1115/1.4048792]

Keywords: finite element modeling, sandwich panel, pyramidal truss, welded joint, modal parameters, operational modal analysis

1 Introduction

Sandwich panels are a type of composite structures and widely used in commercial vehicles and aerospace and military industries. A typical sandwich panel consists of two face sheets that provide bending and in-plane shear stiffnesses, and a core part that carries out-of-plane shear loads. According to types of core parts, sandwich panels can be classified as foams, corrugations, honeycombs, trusses, and so on. Compared with monolithic plate structures and other types of sandwich panels, truss sandwich panels have lower weights but higher stiffnesses and strengths [1,2]. Other physical properties of truss sandwich panels, such as the energy absorption capacity, the heat dissipation capability, and the heat transfer capability, have also been investigated by researchers [3,4].

In this study, modeling of a pyramidal truss sandwich panel (PTSP) is discussed. Various methods used to fabricate PTSPs, such as extrusion and electro-discharge machining [5], three-dimensional (3D) printing [6,7], and interlocking and vacuum-brazing [8,9], have been investigated. As shown in Fig. 1, the core part of the PTSP studied in this work is first manufactured by punching a perforated metallic sheet in a special air die. The second step of this process is to bond face sheets and the pyramidal truss core through the welding technique. As a result, pyramidal unit cells are periodically arrayed in three dimensions. By applying the above manufacturing process, the effect of temperature on material properties is weakened since the truss core is kept as one piece

instead of being bonded together by single beams through the welding process.

Solid elements are generally used in finite element (FE) models of sandwich panels and their high accuracies in static and dynamic analyses have been proved in many investigations. Yang et al. [10] created solid element models of PTSPs to study effects of viscoelastic layers on their vibration and damping performance. Good agreement between numerical and experimental results is reported by them. Li et al. [11] used solid elements to simulate sandwich panels with hourglass truss cores and obtained acceptable differences between numerical and experimental results. However, sandwich panels in above studies were mainly manufactured through the hot press molding technology. In this investigation, welded joints of the PTSP between its face sheets and truss core, as shown in Fig. 2, are made by the welding process. For this kind of sandwich panels, previous studies ignored welded joints in their FE models [12,13]. However, dimensions of joints between face sheets and the core part of a sandwich panel can affect its static and dynamic characteristics [14,15]. Syam et al. [14] designed some strut-based lattice structures and studied their static and dynamic mechanical properties. They found that percentage differences between numerical and experimental results of structural stiffnesses range from 0.8% to 26%. The error analysis indicated that geometrical discrepancies of connecting nodes are one of main reasons of these differences. Yang et al. [15] established a solid element model to investigate modal properties of a sandwich cylindrical panel and compared its simulation and experimental results. A maximum error of 14.6% in natural frequencies and loss of individual modes were reported in their work.

Based on above discussions, one can see that welded joints play an important role in the modeling of sandwich panels. Shapes of welded joints are generally irregular during the fabrication process, but fillets are always used to simulate them in some

---

Journal of Vibration and Acoustics   AUGUST 2021, Vol. 143 / **041002-1**
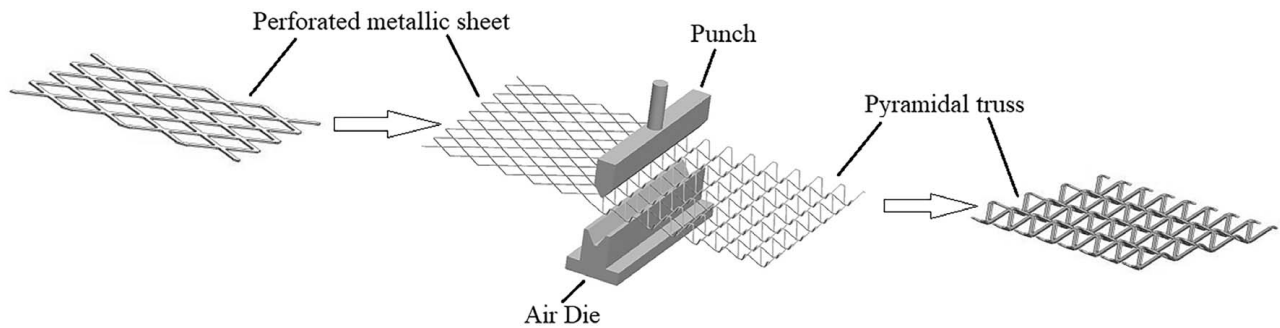
Fig. 1   Manufacturing process of the core part of the PTSP studied in this work

fields, including fatigue assessment of welded joints [16] and flow performance investigation of PTSPs [3]. As shown in Fig. 3, fillets are created between the truss core and face sheets of the solid element model of the PTSP in this work, and dense meshes are applied to it to reduce errors caused by stress concentration when solid elements are used. As a result, much longer computation time and much larger computer memory are needed in the FE analysis, especially for relatively large and complicated structures.

One method to save time and memory in the FE analysis is to use beam and shell elements to model a PTSP with welded joints, which are much more efficient than solid elements, since the number of degrees of freedom (DOFs) in a beam-shell element model is much fewer than that in a solid element model. Some researchers who focus on honeycomb-core sandwich panels usually use shell elements in their FE models due to characteristics of core parts [17,18]. However, Burlayenko and Sadowski [19] suggested that shell elements that save computation time have less accuracy than solid elements in the calculation of natural frequencies of foam-filled honeycomb-core sandwich panels. Their results indicated that natural frequencies were overestimated by 8–10% when shell elements were used in FE models. Simplification of PTSPs is not always as easy as that of honeycomb-core sandwich panels due to the existence of beam members in core parts of the PTSPs. Some researchers created FE models of PTSPs with shell elements in face sheets and solid elements in truss cores to obtain enough accuracy [20,21], but DOFs of the FE models were not significantly reduced. Yuan et al. [13] used beam and shell elements to build FE models of PTSPs and analyzed their buckling behaviors. Zhou and Li [22] detected damage of a PTSP based on its vibration characteristics, and beam and shell elements were used in their FE model of the PTSP. The FE model in their investigation was remarkably simplified; however, local effects of welded joints on the PTSP were not considered in their model. Xu and Deng [23] investigated simplifications of FE models of spot-welded joints and proposed several types of simplified joint models, including the single-bar model, the spoke-bar model, and the multiple rigid-

bar model. Results of the structural stiffness of a joint showed that these simplifications have great accuracy in loading conditions of tension, torsion, and out-of-plane bending, but large errors for in-plane bending and torsion. Most of the above studies focus on static analysis of PTSPs, and more studies on dynamic analysis of PTSPs modeled by beam and shell elements are needed and modal tests of PTSPs need to be improved to resolve the missing mode problem [15].

This work aims to accurately determine modal parameters, including natural frequencies and mode shapes, of a PTSP with welded joints with much fewer DOFs than those of its solid element model and to improve accuracy of modal test results of a PTSP specimen by avoiding the missing mode problem. Two novel methods that consider the stiffness of welded joints created by solid elements as equivalent stiffnesses of beam and shell elements are developed to significantly simplify the solid element model. In these two methods, the equivalent stiffnesses are calculated by matching displacements of welded joints created by beam and shell elements with those created by solid elements. The equivalent stiffness of beam elements is simulated by adding extra beam elements with corresponding cross-sectional dimensions, while the equivalent stiffness of shell elements is simulated by updating their Young's modulus in one method and their thickness in the other method. In operational modal analysis of the PTSP specimen with simulated free boundary conditions, a speaker was used to excite it and a 3D scanning laser vibrometer (SLV) was used to measure its vibration. In order to synchronously capture mode shapes of two face sheets of the specimen, vibration of the backface of the specimen is measured through its image in a mirror and combined with that of its frontface. Novelties of this work are summarized as follows. First, the FE model of a PTSP with welded joints is significantly simplified and its modal parameters are accurately obtained. Second, the missing mode problem in the modal test of the PTSP is resolved by simultaneously measuring vibrations of its two face sheets.

The remainder of this paper is organized as follows. In Sec. 2, based on the directly simplified model of the PTSP created by beam and shell elements with welded joints ignored, two novel methods that consider effects of welded joints as equivalent stiffness are proposed. Methodologies for calculating equivalent parameters of beam and shell elements are developed there. In Sec. 3, modal parameters of the PTSP from the two proposed models and
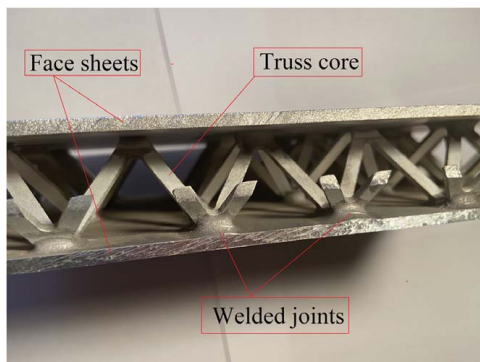

Fig. 2   Components of the PTSP studied in this work with welded joints made by the welding process
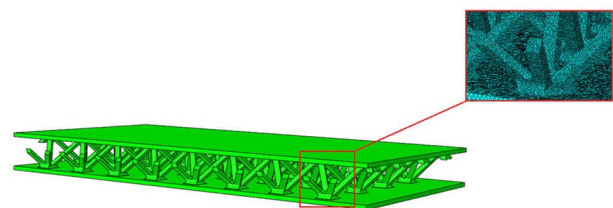

Fig. 3   Solid element model of the PTSP in this work with dense meshes applied to welded joints

the model that ignores welded joints are compared with those from the solid element model to check accuracy of the two proposed models. In Sec. 4, operational modal analysis of the PTSP specimen is conducted by using a 3D SLV to validate modal parameters estimated by the two proposed models and the experimental setup to improve accuracy of experimental results is discussed. Some conclusions are presented in Sec. 5.

2 Methodology

The commercial finite element software ABAQUS is used in this study to build FE models of the PTSP with welded joints. Solid elements C3D4 are used in the solid element model, and beam elements B33 and shell elements S4R are used in beam-shell element models. Natural frequencies and mode shapes of PTSP models with free boundary conditions are extracted through the Lanczos approach [24]. Equal dimensions of welded joints are assumed in numerical calculation.

2.1 Direct Simplification Method. As mentioned in Sec. 1, direct simplification methods have been used to model sandwich panels in some published works [12,13,19]. For the directly simplified beam-shell element model of the PTSP in this study that ignores welded joints, its face sheets can be modeled by shell elements and the truss core can be modeled by beam elements, as shown in Fig. 4. Both material properties and dimensions of the directly simplified model of the PTSP are kept the same as those of the solid element model. Besides, a "tie" is used as the constraint between beam and shell elements in the directly simplified model.

2.2 Equivalent Welded Joint Modeling Methods. Based on the direct simplification method, two novel methods that consider the stiffness of welded joints created by solid elements as equivalent stiffnesses of beam and shell elements are proposed here. Modal parameters, such as natural frequencies and mode shapes, of a structure are mainly determined by its mass and stiffness. The approaches here mainly focus on predicting the equivalent stiffness introduced by welded joints, since the mass of the beam-shell element model of the PTSP can be easily matched with that of its solid element model by updating its density. Material properties or dimensions of beam and shell elements can be correspondingly changed to satisfy the stiffness equivalence. Note that the equivalent mass and stiffness of beam-shell element models of the PTSP are not updated based on experimental data, but are updated based on numerical analysis of its solid element model.

As shown in Fig. 5, a pyramidal truss unit of the solid element model of the PTSP in this work basically consists of a part of a thin face sheet, four beam members, and four fillets at a welded joint. Some researchers have studied effects of fillets and different types of joints on modal parameters of structures. Brown and Seugling [25] studied a thin-walled structure with fillets and modeled a fillet as a "bridge" plate to consider its in-plane effect on modal parameters of the structure. He and Zhu [26] investigated thin-walled beams with fillets and modeled both in-plane and out-of-plane effects of the fillets by matching rotational displacements of a half fillet from the curved beam theory and finite

Fig. 5 Components of a pyramidal truss unit of the solid element model of the PTSP in this work, including a part of a face sheet, four beam members, and four fillets at a welded joint: (a) 3D view and (b) the right side view

element model, and matching area moments of inertia and torsional displacements from the beam theory and finite element model, respectively. He and Zhu [27] developed a novel method for accurately predicting stiffnesses of tightened bolted connections in beams using their contact area radii. Kim et al. [28] developed a linear FE modeling method to accurately estimate modal parameters of joined structures with riveted connections by simulating riveting processes using their nonlinear FE models.

By separating beam members and the face sheet from the welded joint at tangent sections and vertical sections in Fig. 5, the welded joint can be solely analyzed to obtain its stiffness. A single welded joint is shown in Fig. 6, where two orthogonal symmetrical planes can be seen. A quarter of the welded joint with fixed boundaries on the symmetrical planes can be analyzed to obtain the stiffness of the whole joint, since one can assume that there is no deformation on the symmetrical planes.

The stiffness of the welded joint can be decomposed into two parts: the stiffness of beam members and that of the welded joint plate shown in Fig. 5. A beam with a fillet is compared with
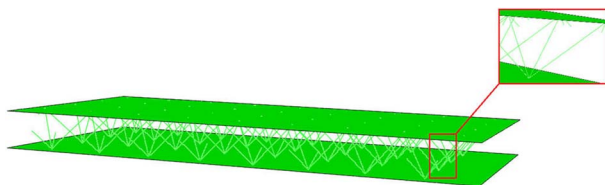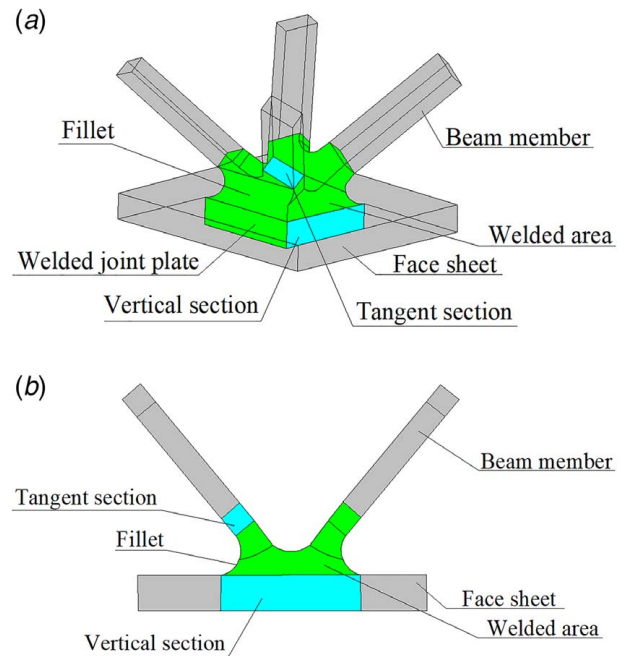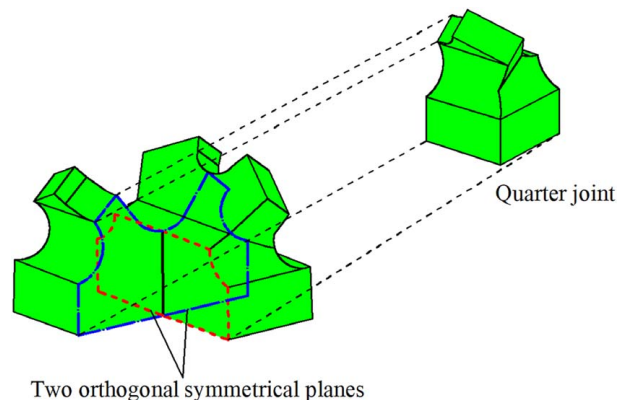

Fig. 4 Directly simplified beam-shell element model of the PTSP in Fig. 3: face sheets are created by shell elements, the truss core is created by beam elements, and welded joints are ignored

Fig. 6 Single welded joint and its quarter part that is cut along its two orthogonal symmetrical planes

that without the fillet in Fig. 7. One can see that the existence of the fillet makes the cross section of the beam variable and leads to its larger equivalent cross-sectional dimensions than those of the corresponding beam without the fillet. Therefore, the equivalent stiffness of the beam becomes larger when the effect of the fillet is considered. Similarly, as shown in Fig. 8, the welded joint increases the equivalent thickness of the plate due to the existence of the fillet and leads to augmentation of the plate stiffness.

In this work, it is assumed that solid elements used in a welded joint can be substituted by sloped beam elements that have the same orientations and cross-sectional dimensions as original beam members in the pyramidal truss unit in Fig. 5, vertical beam elements that offer an extra stiffness, and shell elements that have the equivalent bending stiffness to that of the original plate in the pyramidal truss unit, as shown in Fig. 9. A pin is used to connect the sloped beam and vertical beam, and a concentrated force F and a bending moment M are applied at the pin point, as shown in Fig. 10. Since cross sections of beam elements are rectangles, the equivalent stiffness of vertical beam elements can be calculated under loading conditions in two orthogonal planes referred to the in-plane and out-of-plane, which are the plane formed by the sloped and vertical beams and that perpendicular to it, respectively, as shown in Fig. 10, and the equivalent stiffness of vertical beam elements can be expressed as their cross-sectional dimensions. The predictive modeling procedure for the equivalent out-of-plane stiffness, the equivalent in-plane stiffness, and the equivalent bending stiffness of the beam-shell element model of the welded joint is shown below.

2.2.1 Out-of-Plane Stiffness of Beam Elements. As shown in Fig. 9, the sloped and vertical beams in the quarter welded joint are referred to as beam 1 and beam 2, respectively. When F and M are applied in the out-of-plane, force equilibria of the two beams are shown in Fig. 11, where U_1-V_1 and U_2-V_2 are local

Fig. 8 Comparison of plates with and without the fillet: (*a*) 3D view of a half welded joint cut from a symmetrical plane of the joint, (*b*) the welded joint plate with the fillet, and (*c*) the plate without the fillet; the thickness of the welded joint plate becomes larger due to the existence of the fillet
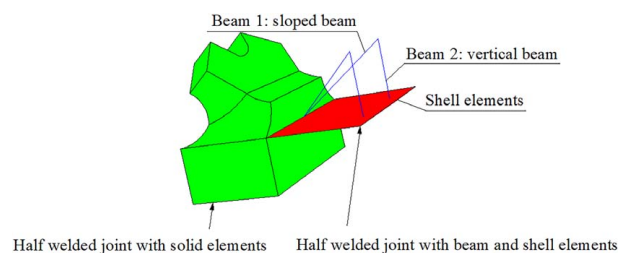
Fig. 9 Equivalent model of a welded joint with sloped beam elements that have the same orientations and cross-sectional dimensions as original beam members in the pyramidal truss unit in Fig. 5, vertical beam members that offer an extra stiffness, and shell elements that have the equivalent bending stiffness to that of the original plate in the pyramidal truss unit
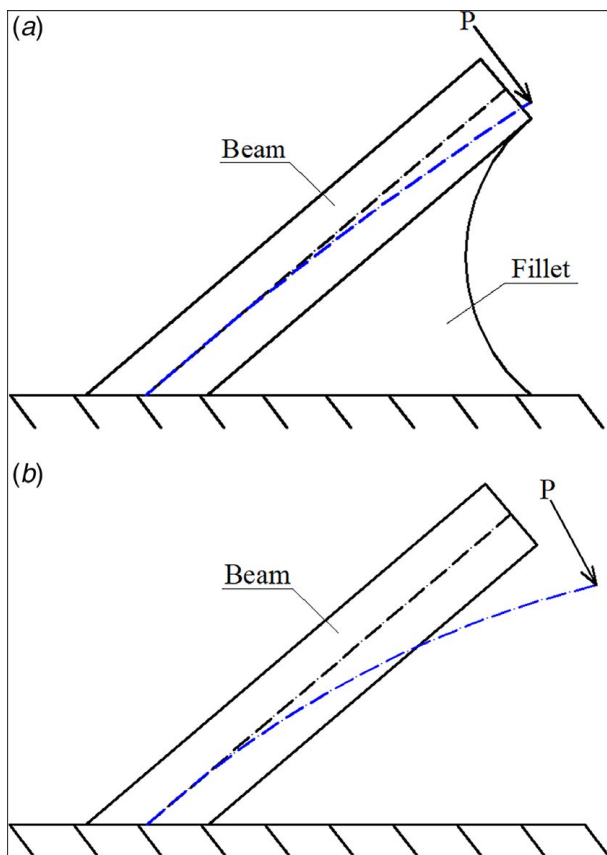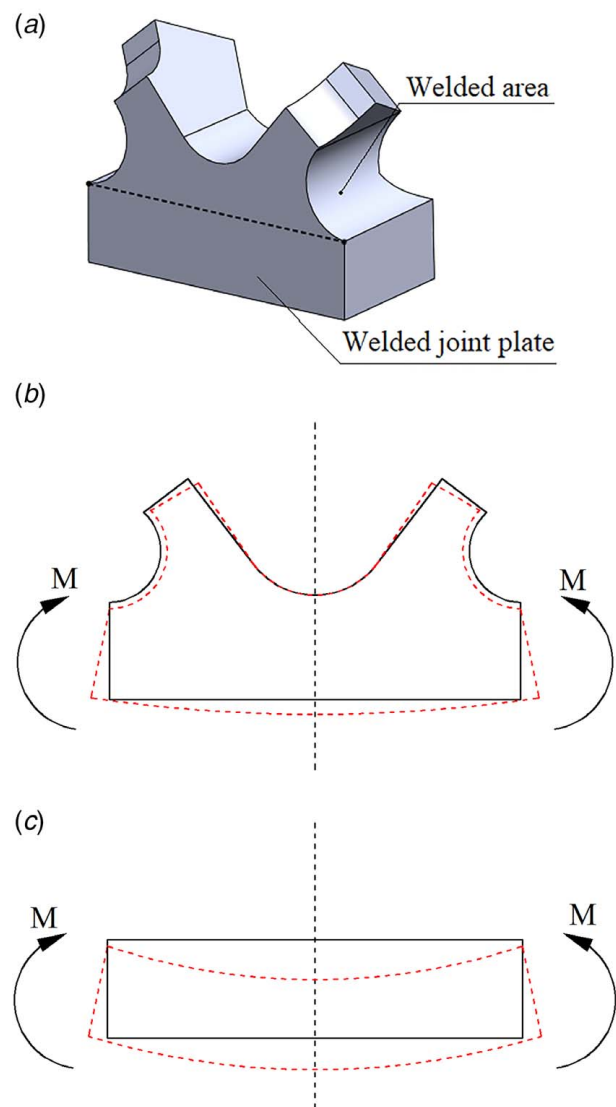

Fig. 7 Comparison of beams (*a*) with and (*b*) without a fillet: the beam cross section in (*a*) varies due to the existence of the fillet

Cartesian coordinates of displacements for beams 1 and 2, respectively, and they can be transformed to each other through a transformation matrix that is a function of the angle α between the two beams. According to the analysis in Fig. 11, relations between loads and beam displacements for beams 1 and 2 can be written as
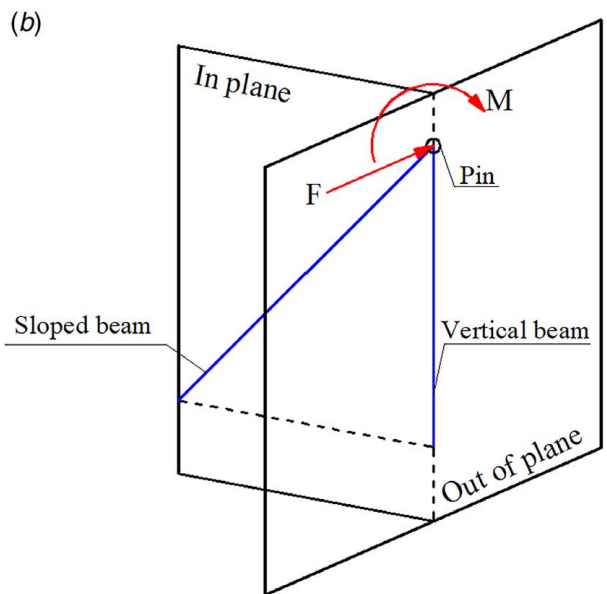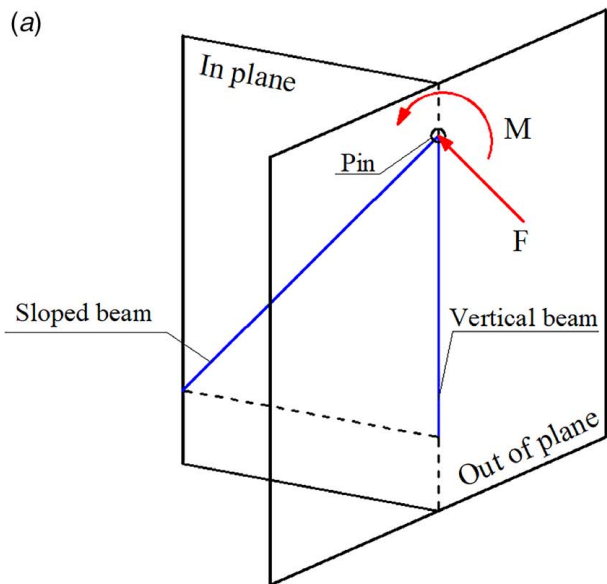
Fig. 10 Beam elements used to calculate the equivalent stiffness of the quarter welded joint: (a) an in-plane concentrated force and a bending moment are applied at the pin and (b) an out-of-plane concentrated force and a bending moment are applied at the pin

Fig. 11 Force equilibria of beams 1 and 2 when the out-of-plane force and moment are applied at the pin
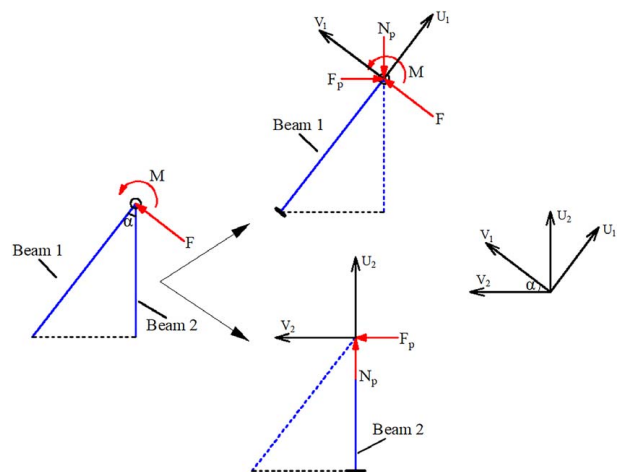
Fig. 12 Force equilibria of beams 1 and 2 when the in-plane force and moment are applied at the pin

$$K_1^{out} \begin{bmatrix} U_1^{out} \\ V_1^{out} \\ \theta_1^{out} \end{bmatrix} = \begin{bmatrix} \dfrac{A_1 E}{L_1} & 0 & 0 \\ 0 & \dfrac{12EI_1^{out}}{L_1^3} & -\dfrac{6EI_1^{out}}{L_1^2} \\ 0 & -\dfrac{6EI_1^{out}}{L_1^2} & \dfrac{4EI_1^{out}}{L_1} \end{bmatrix} \begin{bmatrix} U_1^{out} \\ V_1^{out} \\ \theta_1^{out} \end{bmatrix} = \begin{bmatrix} 0 \\ F - F_p^{out} \\ M \end{bmatrix} \tag{1}$$

$$K_2^{out} \begin{bmatrix} U_2^{out} \\ V_2^{out} \\ \theta_2^{out} \end{bmatrix} = \begin{bmatrix} \dfrac{A_2 E}{L_2} & 0 & 0 \\ 0 & \dfrac{12EI_2^{out}}{L_2^3} & -\dfrac{6EI_2^{out}}{L_2^2} \\ 0 & -\dfrac{6EI_2^{out}}{L_2^2} & \dfrac{4EI_2^{out}}{L_2} \end{bmatrix} \begin{bmatrix} U_2^{out} \\ V_2^{out} \\ \theta_2^{out} \end{bmatrix} = \begin{bmatrix} 0 \\ F_p^{out} \\ 0 \end{bmatrix} \tag{2}$$
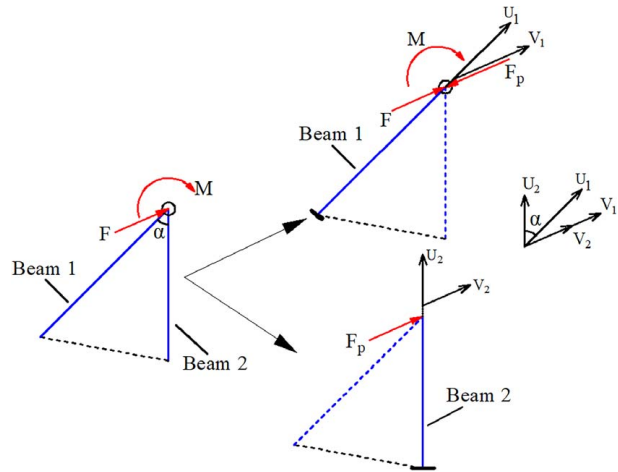

Fig. 13 Coordinate system established on the plane formed by the welded joint plate, and moments applied to it along X and Y directions

respectively, where the superscript "out" denotes out-of-plane, and subscripts "1" and "2" denote beams 1 and 2, respectively; U, V, and θ denote axial, transverse, and rotational displacements of either beam at its end at the pin, respectively; E is the Young's modulus of 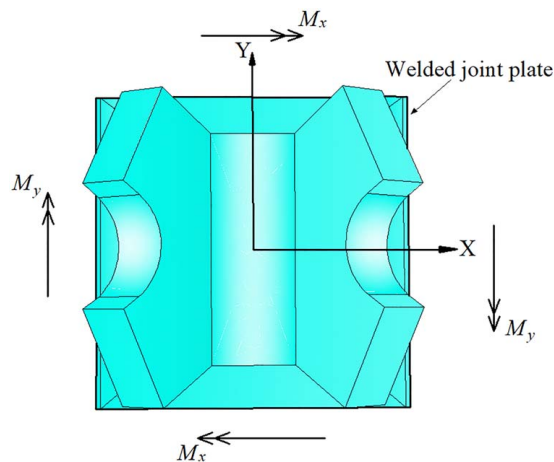the two beams; L, A, and I denote the length, cross-sectional area, and area moment of inertia of a cross section of either beam, respectively; F_p denotes the reaction force on either beam from the pin along the transverse direction of the beam; and K denotes the stiffness matrix of either beam with its components shown there. There is no axial force in either beam when F and M are applied in the out-of-plane. The out-of-plane transverse displacement of beam 1 V_1^{out} is equal to that of beam 2 V_2^{out}. Therefore,

Eqs. (1) and (2) can be simplified as

$$\begin{bmatrix} \dfrac{12EI_1^{out}}{L_1^3} & -\dfrac{6EI_1^{out}}{L_1^2} \\ -\dfrac{6EI_1^{out}}{L_1^2} & \dfrac{4EI_1^{out}}{L_1} \end{bmatrix} \begin{bmatrix} V_1^{out} \\ \theta_1^{out} \end{bmatrix} = \begin{bmatrix} F - F_p^{out} \\ M \end{bmatrix} \quad (3)$$

$$\begin{bmatrix} \dfrac{12EI_2^{out}}{L_2^3} & -\dfrac{6EI_2^{out}}{L_2^2} \\ -\dfrac{6EI_2^{out}}{L_2^2} & \dfrac{4EI_2^{out}}{L_2} \end{bmatrix} \begin{bmatrix} V_1^{out} \\ \theta_2^{out} \end{bmatrix} = \begin{bmatrix} F_p^{out} \\ 0 \end{bmatrix} \quad (4)$$

Since the rotational displacement of a beam affects more its behavior than axial and transverse displacements [16], only θ is selected to match results from above analytical models and the numerical result from the solid element model of the quarter welded joint. In other words, θ_1^{out} in Eqs. (3) and (4) can be calculated from the solid element model of the quarter joint by applying the out-of-plane force and moment to it. As previously mentioned, beam 1 has the same cross section as original beam members in the pyramidal truss unit, which is rectangular and whose dimensions can be directly measured. The out-of-plane area moment of inertia of beam 1 I_1^{out} in Eq. (3) is $th^3/12$, where t and h are its cross-sectional dimensions. The out-of-plane transverse displacement of
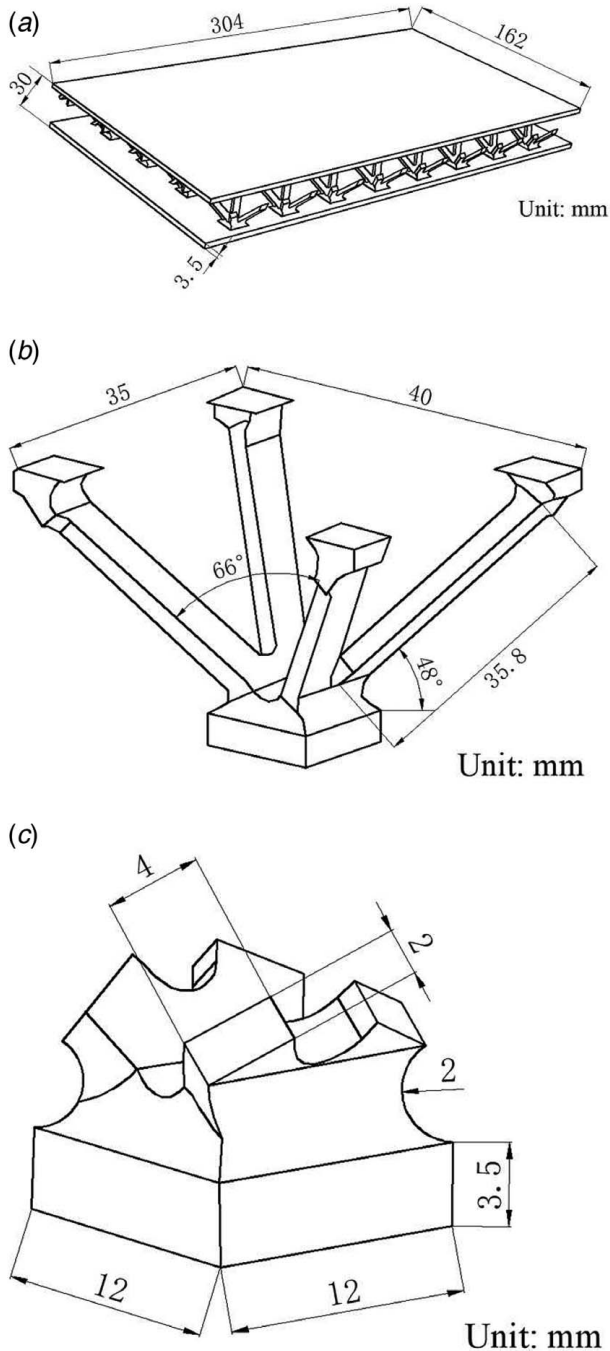
Fig. 14 Dimensions of the solid element model of the PTSP with welded joints: dimensions of (a) the whole PTSP, (b) a pyramidal truss unit, and (c) a welded joint

Fig. 15 (a) Distribution of the out-of-plane rotational displacement of the quarter welded joint from the solid element model when the out-of-plane force and moment are applied to it and (b) that of the in-plane rotational displacement of the quarter welded joint from the solid element model when the in-plane force and moment are applied to it

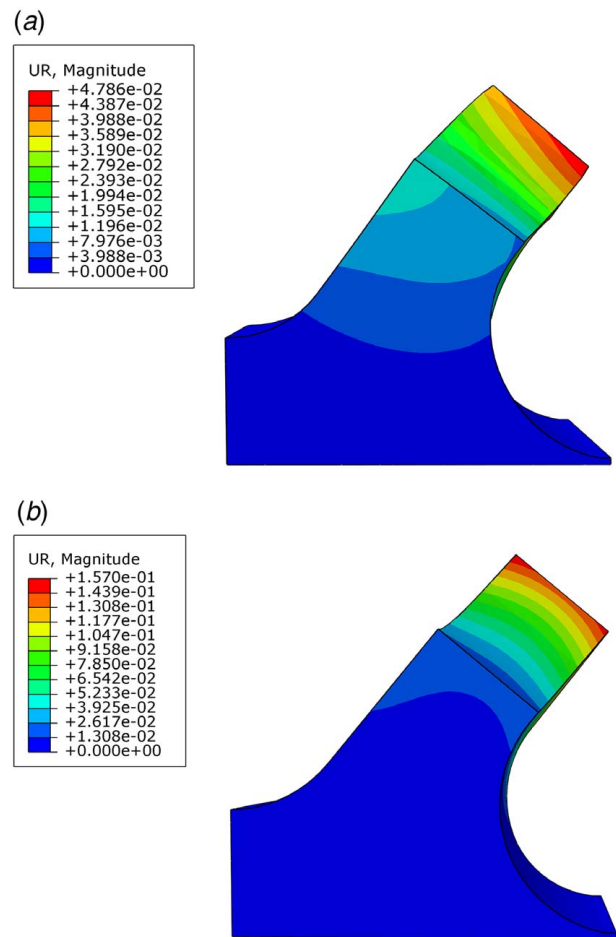beam 1 V_1^{out}, the out-of-plane transverse reaction force F_p^{out}, the out-of-plane moment of inertia of beam 2 I_2^{out}, and the out-of-plane rotational displacement of beam 2 θ_2^{out} are four unknown variables that can be subsequently calculated from four equations in Eqs. (3) and (4).

2.2.2 In-Plane Stiffness of Beam Elements.
Relations between in-plane loads and displacements of beams 1 and 2 can be similarly derived from Fig. 12, which are

$$
K_1^{in}\begin{bmatrix} U_1^{in} \\ V_1^{in} \\ \theta_1^{in} \end{bmatrix} = \begin{bmatrix} \dfrac{A_1 E}{L_1} & 0 & 0 \\ 0 & \dfrac{12EI_1^{in}}{L_1^3} & -\dfrac{6EI_1^{in}}{L_1^2} \\ 0 & -\dfrac{6EI_1^{in}}{L_1^2} & \dfrac{4EI_1^{in}}{L_1} \end{bmatrix} \begin{bmatrix} U_1^{in} \\ V_1^{in} \\ \theta_1^{in} \end{bmatrix}
$$
$$
= \begin{bmatrix} -N_p^{in}\cos\alpha + F_p^{in}\sin\alpha \\ F - N_p^{in}\sin\alpha - F_p^{in}\cos\alpha \\ M \end{bmatrix} \tag{5}
$$

$$
K_2^{in}\begin{bmatrix} U_2^{in} \\ V_2^{in} \\ \theta_2^{in} \end{bmatrix} = \begin{bmatrix} \dfrac{A_2 E}{L_2} & 0 & 0 \\ 0 & \dfrac{12EI_2^{in}}{L_2^3} & -\dfrac{6EI_2^{in}}{L_2^2} \\ 0 & -\dfrac{6EI_2^{in}}{L_2^2} & \dfrac{4EI_2^{in}}{L_2} \end{bmatrix} \begin{bmatrix} U_2^{in} \\ V_2^{in} \\ \theta_2^{in} \end{bmatrix} = \begin{bmatrix} N_p^{in} \\ F_p^{in} \\ 0 \end{bmatrix} \tag{6}
$$

respectively, where in-plane variables have similar meanings to out-of-plane variables previously discussed; N_p^{in} and F_p^{in} are in-plane reaction forces from the pin along axial and transverse directions of beam 2, respectively; I_1^{in} is the in-plane area moment of inertia of beam 1, whose calculation is similar to that of its out-of-plane area moment of inertia; and I_2^{in} and A_2 are given by

$$
I_2^{in} = \frac{1}{12}ab^3 \tag{7}
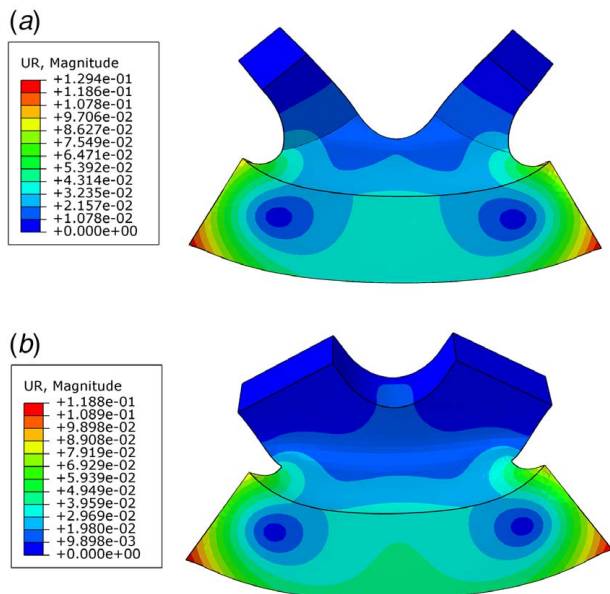$$

$$
A_2 = ab \tag{8}
$$

Fig. 16 Distributions of rotational displacements of edges of the welded joint plate in the solid element model of the whole welded joint when moments are applied along (a) Y and (b) X directions that are defined in Fig. 13

respectively, in which a and b are cross-sectional dimensions of beam 2.

As shown in Fig. 12, transformations between axial and transverse displacements of beams 1 and 2 can be expressed as

$$
U_2^{in} = U_1^{in}\cos\alpha + V_1^{in}\sin\alpha \tag{9}
$$

$$
V_2^{in} = -U_1^{in}\sin\alpha + V_1^{in}\cos\alpha \tag{10}
$$

respectively, where α is the angle between beams 1 and 2. Equations (7)–(10) can be substituted into Eq. (6) to yield

$$
\begin{bmatrix} \dfrac{abE}{L_2} & 0 & 0 \\ 0 & \dfrac{Eab^3}{L_2^3} & -\dfrac{Eab^3}{2L_2^2} \\ 0 & -\dfrac{Eab^3}{2L_2^2} & \dfrac{Eab^3}{3L_2} \end{bmatrix} \begin{bmatrix} U_1^{in}\cos\alpha + V_1^{in}\sin\alpha \\ -U_1^{in}\sin\alpha + V_1^{in}\cos\alpha \\ \theta_2^{in} \end{bmatrix} = \begin{bmatrix} N_p^{in} \\ F_p^{in} \\ 0 \end{bmatrix}
$$
$$
\tag{11}
$$

Note that the out-of-plane moment of inertia of beam 2 I_2^{out} has been previously obtained; the relation between I_2^{out} and a and b is
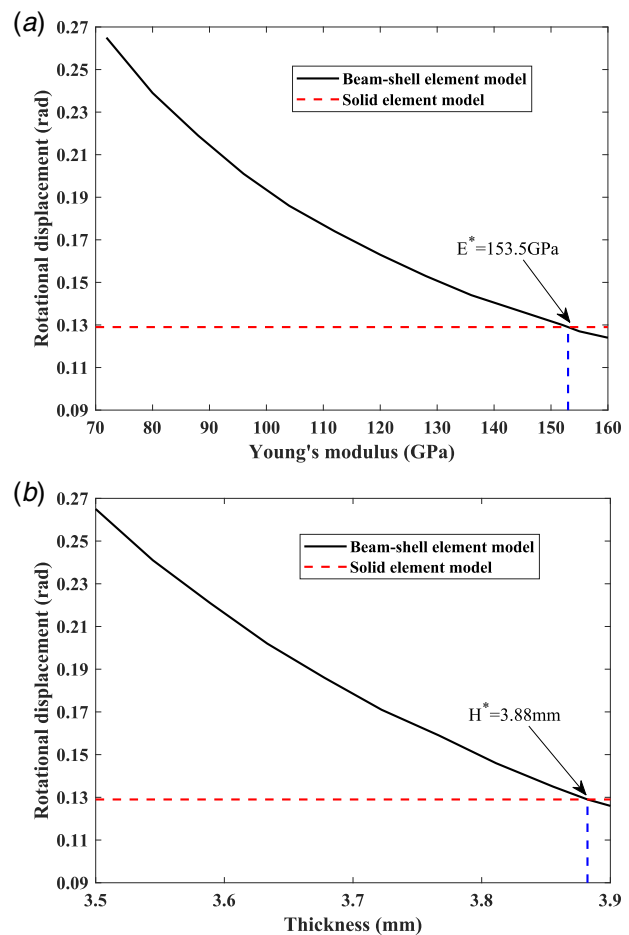
$$
I_2^{out} = \frac{1}{12}ba^3 \tag{12}
$$

Fig. 17 Relation curves between rotational displacements of edges of beam-shell element models of the whole welded joint and (a) the Young's modulus and (b) thickness of shell elements, where horizontal dashed lines denote the rotational displacement of the solid element model of the whole welded joint that is obtained from Fig. 16(a)

Table 1 Young's moduli, cross-sectional dimensions, and thicknesses of beam and shell elements in FE models created by Methods I, II, and III

Method	Beam elements of beam 1		Beam elements of beam 2		Shell elements in welded joints		Shell elements in face sheets	
	E (GPa)	$a \times b$ (mm)	E (GPa)	$a \times b$ (mm)	E (GPa)	H (mm)	E (GPa)	H (mm)
I	71.9	2×4	/	/	/	/	71.9	3.5
II	71.9	2×4	71.9	0.13×8.54	153.5	3.5	71.9	3.5
III	71.9	2×4	71.9	0.13×8.54	71.9	3.9	71.9	3.5
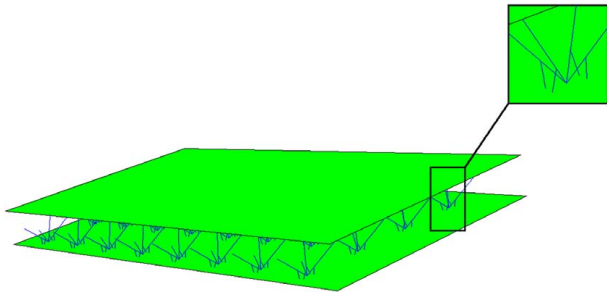
Fig. 18 Beam-shell element model of the PTSP created by Method II or III

Similar to calculating the out-of-plane rotational displacement of beam 1 θ_1^{out}, θ_1^{in} that is the in-plane rotational displacement of beam 1 can be calculated from the solid element model of the quarter welded joint by applying the in-plane force and moment to it. Therefore, the seven unknown variables a, b, N_p^{in}, F_p^{in}, U_1^{in}, V_1^{in}, and θ_2^{in} can be solved from seven equations in Eqs. (5), (11), and (12).

2.2.3 Bending Stiffness of Shell Elements. As shown in Fig. 13, a Cartesian coordinate system X–Y is created on the plane that is formed by the welded joint plate. In order to calculate the equivalent stiffness of shell elements in the welded joint, the first step is to calculate the bending stiffness of the welded joint plate by applying a couple M_x along the X direction and another couple M_y along the Y direction to it. Rotational displacements of the welded joint plate can be calculated from the solid element model of the whole welded joint to determine its bending stiffness. The second step is to create a beam-shell element model of the whole welded joint, where cross-sectional dimensions of vertical beam elements a and b are previously obtained, and to apply M_x and M_y to it. By updating the Young's modulus or thickness of shell elements, rotational displacements of the beam-shell element model of the welded joint can be matched with those of its solid element model. The updated Young's modulus or thickness of shell elements can be used to represent the equivalent bending stiffness of shell elements in welded joints of the whole PTSP created by beam and shell elements.

Based on above analyses and the matching process, the proposed methods can be generally used to simplify the solid element model of a PTSP with welded joints. One can see that parameters of beam and shell elements in the simplified FE model of the PTSP, including their cross-sectional dimensions, Young's modulus, and thickness, are determined by geometrical sizes of its welded joints. Only solid element models of welded joints instead of the whole PTSP would be created. Steps of the proposed methods are measuring geometrical sizes of welded joints in the PTSP, creating solid element models of welded joints, calculating parameters of beam and shell elements through the proposed methods, and creating the beam-shell element model of the whole PTSP. The proposed

methods are numerically verified in Sec. 3 and experimentally validated in Sec. 4.

3 Results of Numerical Analysis

The material and dimensions of the PTSP in numerical analysis correspond to those of the actual PTSP specimen in Sec. 4; the material is aluminum that has a Young's modulus of 71.9 GPa, a density of 2700 kg/m³, and a Poisson's ratio of 0.33. Dimensions of the solid element model of the PTSP are shown in Fig. 14. A face sheet of the PTSP has a length of 304 mm, a width of 162 mm, and a thickness of 3.5 mm. The distance between two face sheets is 30 mm. The distance between ends of two adjacent
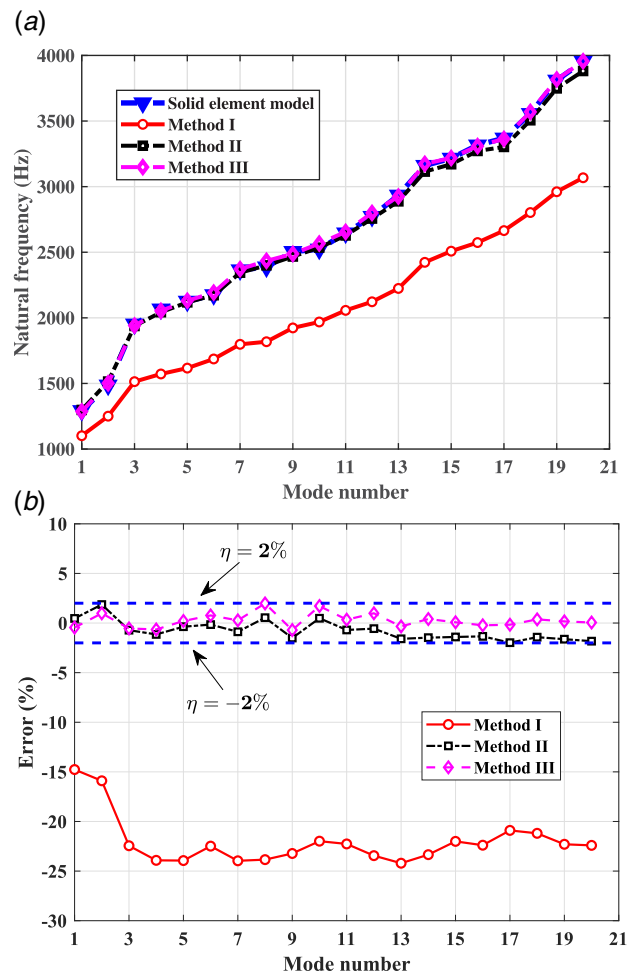
Fig. 19 (a) Natural frequencies of the first 20 elastic modes of the PTSP from its beam-shell element models in Methods I, II, and III and its solid element model and (b) errors between natural frequencies from beam-shell element models and the solid element model
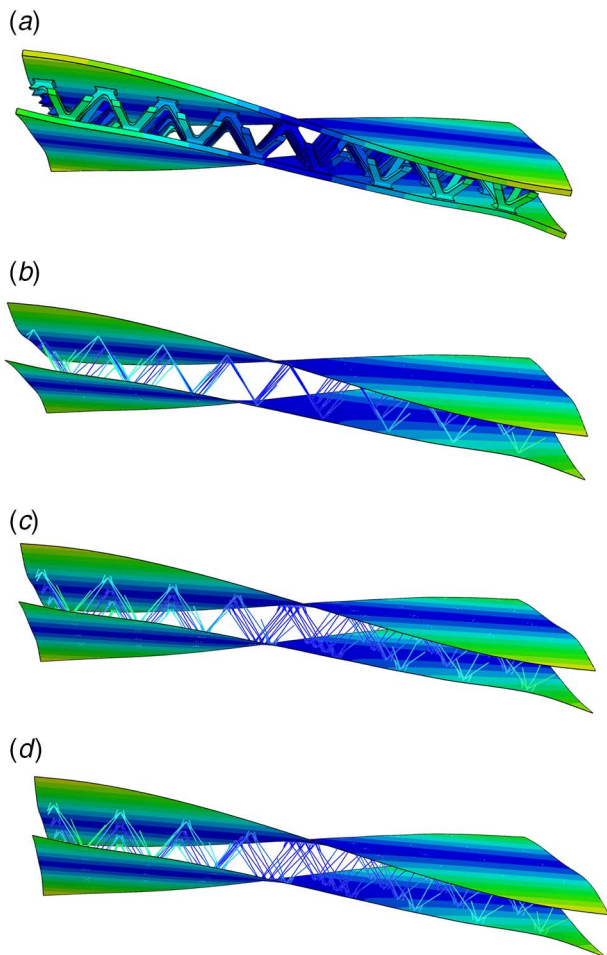
(a)

(b)

(c)

(d)

Fig. 20 First elastic mode shapes from (a) the solid element model, (b) the beam-shell element model in Method I, (c) the beam-shell element model in Method II, and (d) the beam-shell element model in Method III
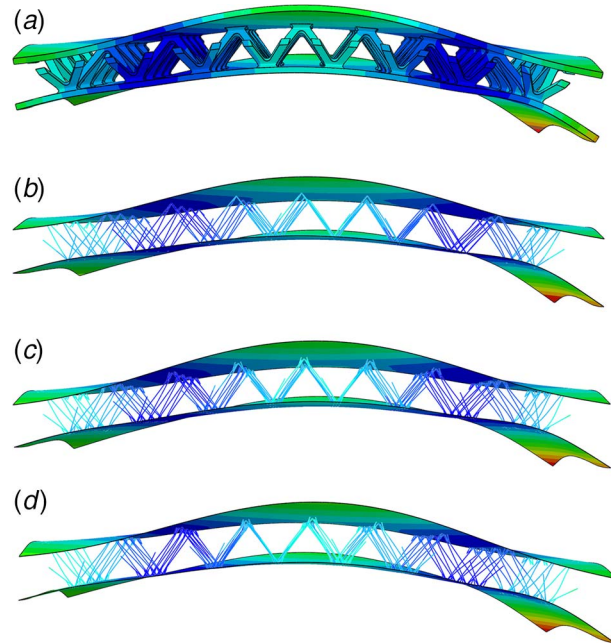

(a)

(b)

(c)

(d)

Fig. 21 Second elastic mode shapes from (a) the solid element model, (b) the beam-shell element model in Method I, (c) the beam-shell element model in Method II, and (d) the beam-shell element model in Method III

beams in a pyramidal truss unit is 35 mm along the length direction of face sheets and 40 mm along their width direction; the total number of pyramidal truss units is 8×4. As shown in Fig. 14(b), the angle between two beams along the width direction of face sheets, which is determined by the air die shown in Fig. 1, is 66 deg. Based on dimensions of the pyramidal truss unit, the relative density of the PTSP in this work can be calculated by [29]

$$\bar{\rho} = \frac{2\pi}{\cos^2 \omega \sin \omega} \left(\frac{t_1}{l}\right)\left(\frac{t_2}{l}\right) \qquad (13)$$

where t_1 and t_2 are cross-sectional dimensions of beam members, l is the length of the beam members, and ω is the angle between the beam members and face sheets. Values of above parameters are shown in Fig. 14 and $\bar{\rho}$ is 11.8% in this work. One can see from Fig. 14(c) that dimensions of the welded joint plate are 12 mm × 12 mm × 3.5 mm, the radius of fillets is 2 mm, and cross-sectional dimensions of beam members are 4 mm × 2 mm, which are approximate dimensions of welded joints in the actual PTSP specimen. As mentioned in Sec. 2, dimensions of all welded joints are assumed to be the same in numerical calculation.

3.1 Results of the Equivalent Stiffness of Beam Elements.
As discussed in Sec. 2, out-of-plane and in-plane bending moments of 10 N·m and concentrated forces of 1000 N are applied to the solid element model of the quarter welded joint to calculate cross-sectional dimensions of beam 2. Lengths of beams 1

and 2 in Fig. 9 are 6 mm and 4.3 mm, respectively. As shown in Fig. 15, out-of-plane and in-plane rotational displacements of beam 1 are $\theta_1^{out} = 0.0479$ rad and $\theta_1^{in} = 0.157$ rad, respectively. As derived in Eqs. (1)–(12), out-of-plane and in-plane moments of inertia of beam 2 can be calculated as $I_2^{out} = 6.8041 \times 10^{-12}$ m^4 and $I_2^{in} = 1.6061 \times 10^{-15}$ m^4, respectively. Therefore, cross-sectional dimensions of beam 2 are $a = 1.3118 \times 10^{-4}$ m and $b = 8.538 \times 10^{-3}$ m. By inputting calculated cross-sectional dimensions of beam 2, a beam-shell element model of the whole welded joint can be created.

3.2 Results of the Equivalent Stiffness of Shell Elements.
As mentioned in Sec. 2, couples M_x and M_y along X and Y directions, respectively, which have the same value of 100 N·m, are applied to the solid element model of the whole welded joint to calculate its rotational displacements. As shown in Fig. 16, rotational displacements of edges of the welded joint plate are 0.129 rad and 0.119 rad along Y and X directions, respectively. It is important to note that equivalent bending stiffnesses of shell elements along the two directions should be separately calculated by matching rotational displacements between the beam-shell element model of the whole welded joint and its solid element model since they are generally different along the two directions; orthotropic elastic properties of shell elements can then be specified by setting their
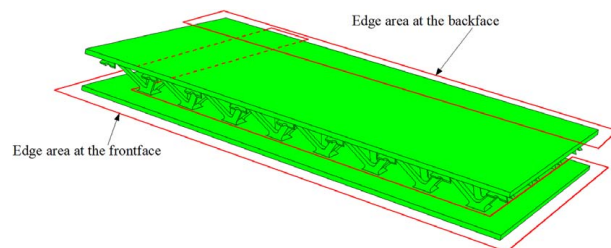

Edge area at the backface

Edge area at the frontface

Fig. 22 Edge areas at the frontface and backface of the PTSP that are not reinforced by the truss core
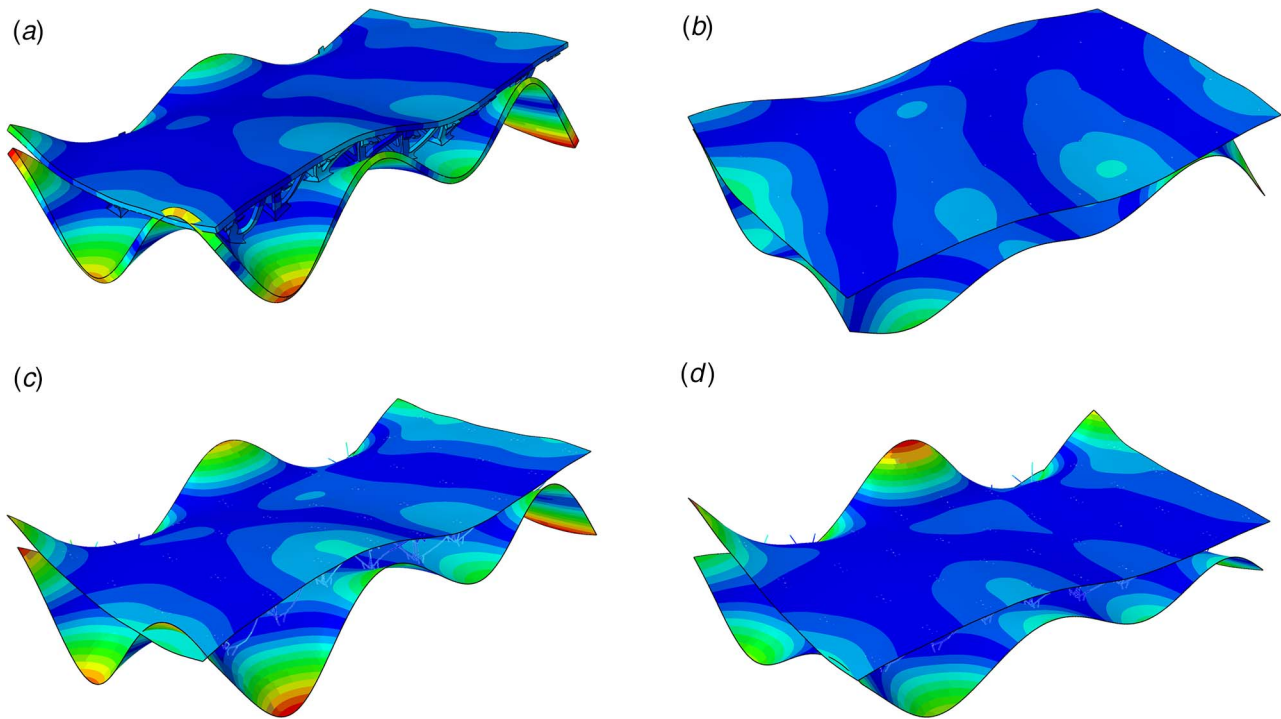
Fig. 23 17th elastic mode shapes from (*a*) the solid element model, (*b*) the beam-shell element model in Method I, (*c*) the beam-shell element model in Method II, and (*d*) the beam-shell element model in Method III

engineering constants in ABAQUS. For this study, however, differences between rotational displacements of the welded joint plate along the two directions are relatively small. Therefore, only the rotational displacement of the welded joint plate along the Y direction is used in calculation of the equivalent bending stiffness of shell elements.

In order to match the rotational displacement of edges of the beam-shell element model of the whole welded joint with that of edges of the welded joint plate in its solid element model, updating the Young's modulus or thickness of shell elements is used as two methods in this work. The initial Young's modulus and thickness of shell elements are the same as those of solid elements. Relation curves between rotational displacements of edges of beam-shell element models of the whole welded joint and the Young's modulus and thickness of shell elements are shown in Fig. 17, where horizontal dashed lines denote the rotational displacement of edges of the welded joint plate in the solid element model of the whole welded joint that is obtained from Fig. 16(*a*). Intersections of relation curves and dashed lines in Fig. 17 denote points where rotational displacements of edges of beam-shell element models of the whole welded joint match those of edges of the welded joint plate in its solid element model. One can see from Fig. 17 that the updated Young's modulus and thickness at intersections of relation curves and dashed lines are $E^*=153.5$ GPa and $H^*=3.88$ mm, respectively.

Beam-shell element models of the PTSP can be created by inputting parameters of beam and shell elements in Table 1 that are obtained from the above numerical analysis, where H is the thickness of shell elements. Methods I, II, and III in Table 1 represent the direct simplification method, the updating Young's modulus method, and the updating thickness method, which are used to create beam-shell element models of the PTSP. One can see that the Young's modulus and cross-sectional dimensions of beam elements of beam 1, and the Young's modulus and thickness of shell elements in face sheets in the three methods are the same as those in the solid element model of the PTSP. Parameters of beam elements of beam 2 and shell elements in welded joints vanish in Method I since welded joints are neglected there. It is noted from Table 1

that Methods II and III have the same cross-sectional dimensions of beam elements of beam 2, which are calculated in Sec. 3.1, but different Young's moduli and thicknesses of shell elements in welded joints, which are obtained in Sec. 3.2.

The beam-shell element model of the PTSP created by Method II or III is shown in Fig. 18. The total number of DOFs of the solid element model of the PTSP that is shown in Fig. 3 is 6,853,806, that of its beam-shell element model created by Method I is 159,648, and that of its beam-shell element model created by Method II or III is 162,912. This indicates that compared with the solid element model of the PTSP, DOFs are reduced by 97.7% for its beam-shell element models in Methods I, II, and III. Compared with DOFs of the solid element model of a welded joint, those of beam-shell element models of the welded joint in Methods II and III are reduced by 99.1%.

3.3 Comparison of Natural Frequencies. Note that the first six modes of FE models of the PTSP in this work are rigid-body modes due to its free boundary conditions; by ignoring rigid-body modes whose natural frequencies are almost zero, only elastic modes that begin with the seventh mode are discussed here. Errors between the ith natural frequencies of beam-shell element models in Methods I, II, and III and that of the solid element model can be calculated by

$$\eta_i^{\text{Method } X} = \frac{f_i^{\text{Method } X} - f_i^{\text{Solid}}}{f_i^{\text{Solid}}} \times 100\% \qquad (14)$$

where the subscript i denotes the ith elastic mode, which ranges from 1 to 20 in this work after ignoring rigid-body modes; superscripts Method X and Solid denote values corresponding to beam-shell element models in Method I, II, or III and that from the solid element model, respectively; and f denotes the corresponding natural frequency.

Natural frequencies of the first 20 elastic modes of the PTSP from its beam-shell element models in Methods I, II, and III are compared with those from its solid element model in Fig. 19. It can be seen
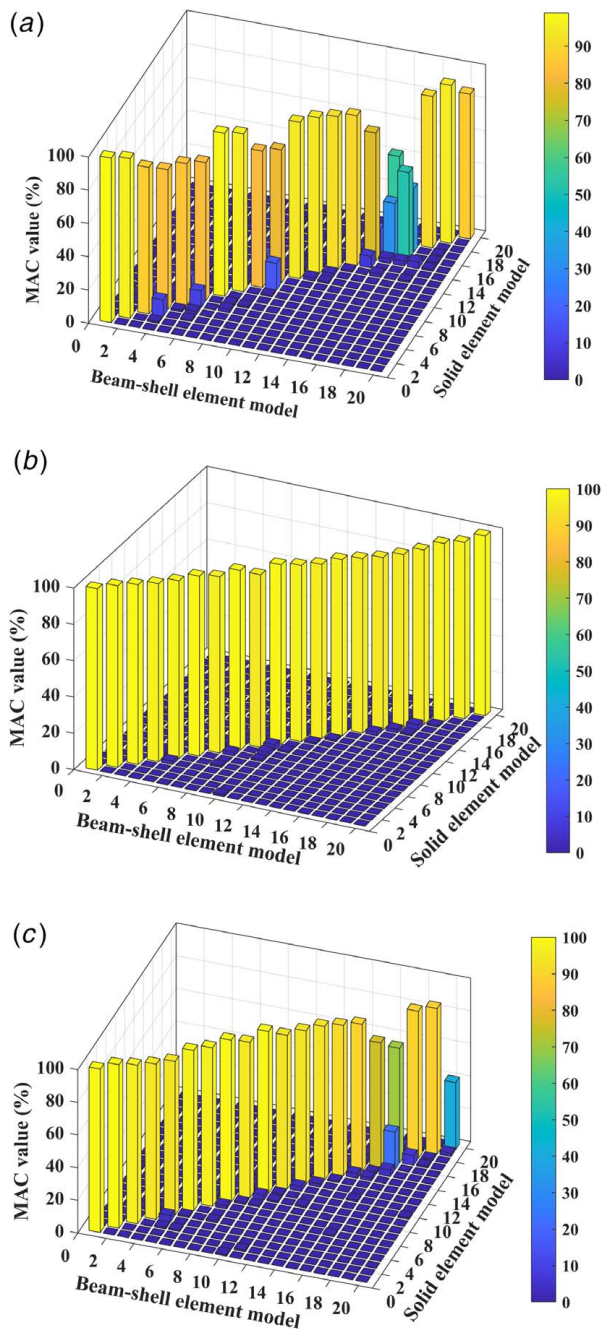
Fig. 24 MAC matrices between mode shapes from the solid element model of the PTSP and those from its beam-shell element models in Methods (*a*) I, (*b*) II, and (*c*) III

those in Method I because welded joints are ignored in Method I, its elastic natural frequencies calculated by Methods II and III are at least 14% more accurate than those by Method I.

In order to demonstrate the necessity of creating beam 2 in Methods II and III, another beam-shell element model of the PTSP, which combines the direct simplification method and equivalent stiffness method, is created and compared with its solid element model. In this equivalent direct simplification method, the beam-shell element model of a welded joint is created to obtain its equivalent stiffness, which is similar to the process in Sec. 2.2, but beam 2 is removed and cross-sectional dimensions of beam 1 are changed from 2 mm × 4 mm to 5.8 mm × 10.8 mm to match the stiffness of the welded joint. The maximum error between the first 20 elastic natural frequencies of the PTSP from its beam-shell element model in the equivalent direct simplification method and those from its solid element model is 6.5%, which is much larger than those in Methods II and III. Therefore, it would be good to obtain the accurate equivalent stiffness of the welded joint by creating an extra beam.

3.4 Comparison of Mode Shapes. The first 20 elastic mode shapes of the PTSP from its four FE models are also compared. The first elastic mode shapes of the PTSP from the four FE models are torsional modes, as shown in Fig. 20, and the second elastic mode shapes from the four models are bending modes, as shown in Fig. 21. Note that the first two elastic modes of the PTSP are global modes, and its two face sheets have almost the same shapes. According to the discussion in Sec. 3.3, Method I that ignores welded joints underestimates both torsional and bending stiffnesses of the PTSP.

Due to the dimensional limitation of the core part in the manufacturing process, edge areas of the PTSP marked in Fig. 22 that are not reinforced by the truss core are located at asymmetric positions of its frontface and backface. As a result, mode shapes of the PTSP from the third through 20th elastic modes are localized mode shapes in these edge areas and asymmetric for the two face sheets, which differ from the first two elastic mode shapes in Figs. 20 and 21. The 17th elastic mode shapes from the four FE models in Fig. 23 show typical high localized mode shapes of the PTSP. It can be seen from Fig. 23 that the frontface and backface of the solid element model of the PTSP have different shapes, and large vibrations occur in its edge areas shown in Fig. 22. The 17th elastic mode shape from the beam-shell element model in Method I is significantly different from that from the solid element model. However, the 17th mode shapes from beam-shell element models in Methods II and III are similar to that from the solid element model. Especially, the 17th mode shape from the beam-shell element model in Method II is in excellent agreement with that from the solid element model.

In order to quantitatively evaluate correlation between mode shapes of the PTSP from its beam-shell element models and solid element model, modal assurance criterion (MAC) values are introduced and can be calculated by

$$MAC_{i,j} = \frac{|(\psi_i^{\text{Solid}})^{\text{H}}(\psi_j^{\text{Method } X})|^2}{[(\psi_i^{\text{Solid}})^{\text{H}}(\psi_i^{\text{Solid}})][(\psi_j^{\text{Method } X})^{\text{H}}(\psi_j^{\text{Method } X})]} \times 100\% \quad (15)$$

where subscripts i and j denote the ith and jth elastic modes, respectively, which range from 1 to 20; the superscript H denotes conjugate transpose of a vector or matrix; and ψ_i and ψ_j denote the ith and jth components of a mode shape vector, respectively. Correlation between mode shapes from beam-shell element models in Methods I, II, and III and those from the solid element model is high for the same modes when MAC values along the diagonal of the MAC matrix are close to 100%, and it is low for different modes when MAC values for off-diagonal elements of the matrix are close to 0 [30].

from Fig. 19(*a*) that elastic natural frequencies from the beam-shell element model in Method I are much smaller than those from the solid element model and differences between them become more significant for the third and higher elastic modes. One can see from Fig. 19(*b*) that absolute values of errors between elastic natural frequencies from the beam-shell element model in Method I and those from the solid element model are about 15% for the first two elastic modes, and they range from 20% to 25% for the third through 20th elastic modes. When Methods II and III are used to create FE models, however, elastic natural frequencies from beam-shell element models are within ±2% of those from the solid element model. While DOFs of beam-shell element models of the PTSP in Methods II and III are 2% larger than
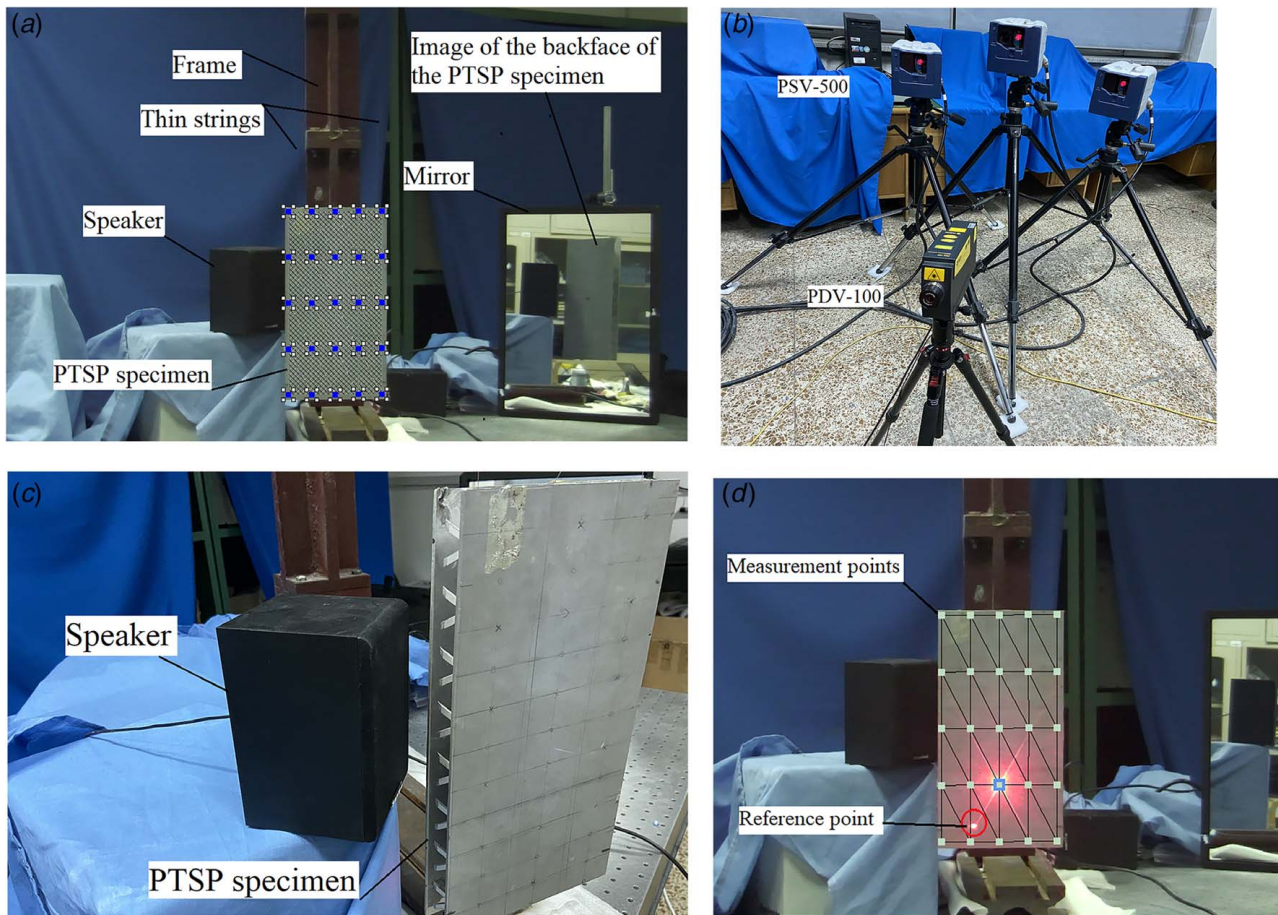
Fig. 25 (*a*) Experimental setup for an operational modal analysis of a PTSP specimen: a speaker was used to excite the specimen, a mirror was used to capture vibration of the backface of the specimen, and two thin strings and a stable heavy frame were used to hang the specimen; (*b*) a 3D SLV PSV-500 with three scanning heads used to measure vibration of the specimen and a single-point laser vibrometer PDV-100 used as a reference measurement; (*c*) the relative position of the speaker to the specimen, which can excite localized mode shapes of the specimen in its edge areas; and (*d*) measurement points on the specimen, which form a 5 × 5 grid on either face sheet of the specimen, and a reference measurement point on the specimen that is selected by avoiding nodal lines of the first 20 elastic modes of the specimen

MAC values between mode shapes from beam-shell element models in Methods I, II, and III and those from the solid element model are shown in Fig. 24. By using Method I to create the beam-shell element model of the PTSP, diagonal MAC values in Fig. 24(*a*) are lower than 90% for some modes and even decrease to about 40% for the 16th and 17th elastic modes, which is consistent with results of the 17th elastic mode shape in Fig. 23. One can see from Fig. 24(*b*) that MAC values between mode shapes from the beam-shell element model in Method II and those from the solid element model are all larger than 95% along the diagonal of the MAC matrix and close to 0 for off-diagonal elements of the matrix. Note that while it is not shown here, absolute values of errors between the 21st through 23rd elastic natural frequencies of the PTSP from its beam-shell element model in Method II and those from its solid element model are 1.8%, 2.4%, and 2.7%, respectively, and corresponding diagonal MAC values between their 21st through 23rd elastic mode shapes are 97%, 99%, and 88%, respectively. This indicates that Method II can provide good results of modal parameters of the PTSP for at least its first 22 elastic modes. While most diagonal MAC values are larger than 95% for the beam-shell element model in Method III, as shown in Fig. 24(*c*), diagonal MAC values decrease to about 70% for the 17th mode and even 40% for the 20th mode, which show weaker correlation between some high mode shapes from the beam-shell element model in Method III and those from the solid element model. A possible reason for this is that updating

the thickness of shell elements in welded joints of the PTSP in Method III leads to thickness discontinuities of face sheets, which may affect some high mode shapes. As shown in Table 1, shell elements in welded joints have a larger thickness than those in other areas of face sheets that do not have welded joints in Method III. While the equivalent stiffness of shell elements in the beam-shell element model of a welded joint in Method III matches that of the plate in its solid element model, nonuniformity of face sheets with different thicknesses may affect some high mode shapes.

4 Experimental Validation of Beam-Shell Element Models in Methods II and III

4.1 Experimental Setup. An operational modal analysis was conducted using a noncontact measurement technique to measure natural frequencies and mode shapes of a PTSP specimen to validate its beam-shell element models in Methods II and III, with the experimental setup shown in Fig. 25. A speaker was used to excite the PTSP specimen, a 3D SLV Polytec PSV-500 with three scanning heads was used to measure 3D responses of measurement points on its two face sheets for capturing their possible 3D mode shapes, and a portable single-point laser vibrometer Polytec PDV-100 was used as a reference measurement. Two thin strings were symmetrically tied to the truss core of the specimen, and the
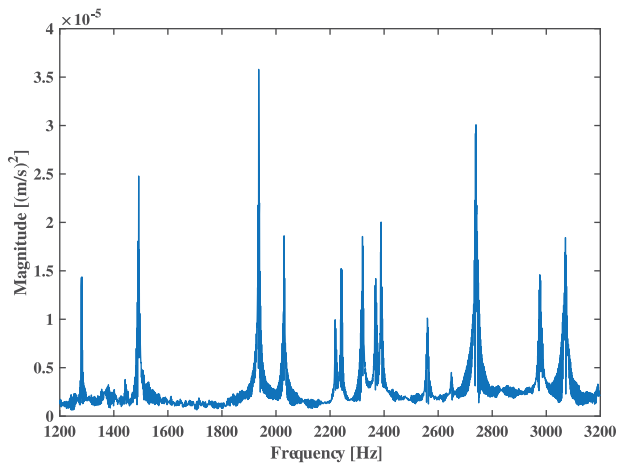
Fig. 26 Sum of cross-power spectra between measurement points and the reference measurement point: 14 peaks can be seen in the selected frequency range and each peak indicates an elastic mode of the specimen

specimen was hung by the strings on a stable heavy frame, which simulated free boundary conditions of the specimen.

As discussed in Sec. 3, except for the first two global elastic modes, the third through 20th elastic modes of the PTSP are localized elastic modes in edge areas of its frontface and backface and
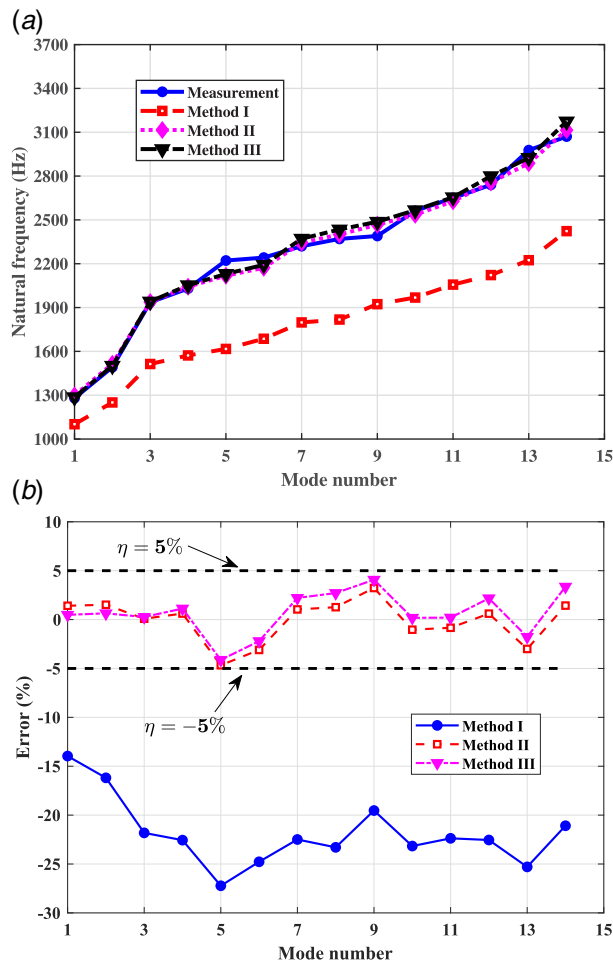

Fig. 27 (a) First 14 elastic natural frequencies of the specimen from its beam-shell element models in Methods I, II, and III and the experiment and (b) errors between these elastic natural frequencies from the beam-shell element models and experiment
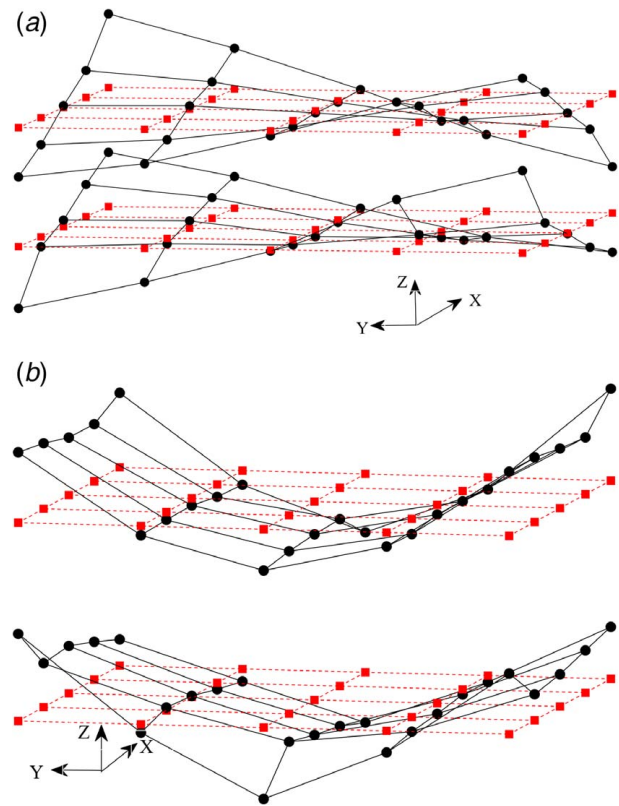

Fig. 28 First two elastic mode shapes of the specimen from the experiment: global (a) torsional and (b) bending modes, respectively

have different shapes for the two face sheets. In order to avoid missing modes of the specimen in operational modal analysis, especially for its high localized modes, some testing strategies were adopted to simultaneously excite and measure global and localized modes of its two face sheets in the experiment. The speaker that was used in the experiment has a relatively small power but a relatively wide bandwidth, so that both low and high elastic modes of the specimen can be excited. The speaker was placed at a side of the specimen instead of placing it in front or at back of its face sheets, as shown in Fig. 25(c), to simultaneously excite modes of the two face sheets. Another significant strategy to avoid missing modes of the specimen was to synchronously measure vibrations of its two face sheets. Since it is required to fix positions of the three scanning heads of the 3D SLV, the single-point laser vibrometer, and the specimen during the experiment, a mirror was used to synchronously measure vibration of its backface, which is essential for two-faced vibration measurement. One can see from Fig. 25(a) that vibrations of measurement points on the frontface of the specimen were directly measured and those on its backface were synchronously measured through their images in the mirror.

A total number of 50 measurement points were selected in this experiment, which formed a 5×5 grid on either face sheet of the specimen, as shown in Fig. 25(d). To avoid selecting the location of the reference measurement point on nodal lines of elastic modes of the specimen, its first 20 elastic mode shapes from its solid element model or beam-shell element model in Method II in Sec. 3 were used to determine the location of the reference measurement point, as shown in Fig. 25(d). A periodic chirp signal from the 3D SLV was inputted into the speaker as the source signal. A rectangular window and three-time spectrum averaging were used in the experiment to minimize errors from leakage and noise. With a sampling frequency of 8000 Hz and a bandwidth of 3200 Hz, each set of vibration data at all measurement points on the two
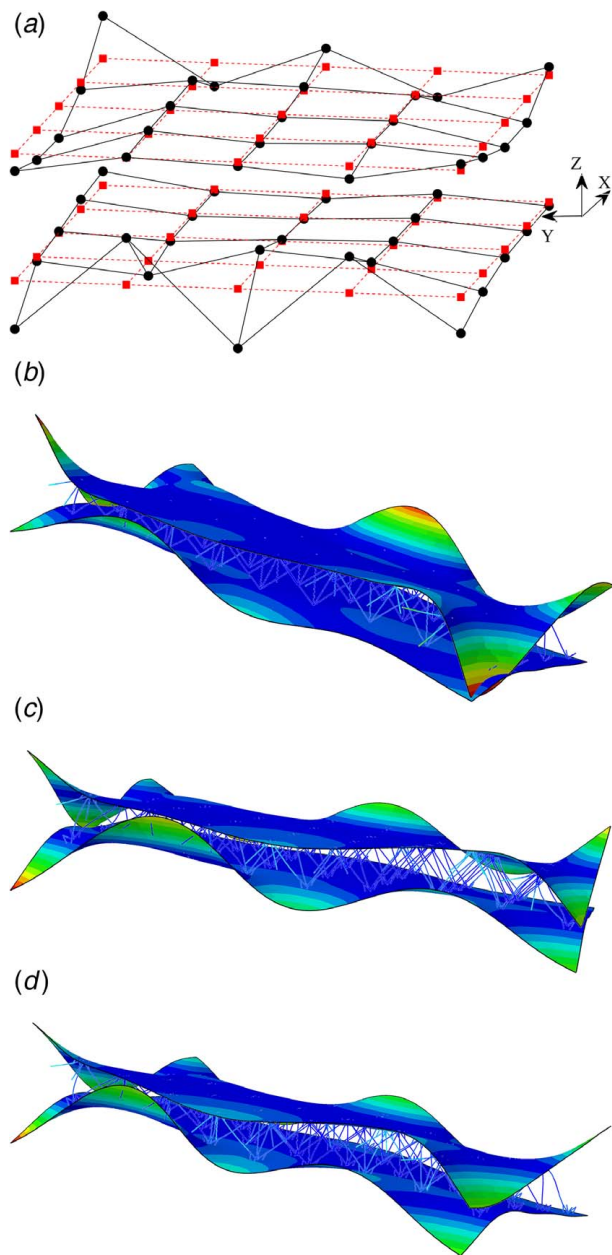
Fig. 29 14th elastic mode shapes from (*a*) the experiment, (*b*) the beam-shell element model in Method I, (*c*) the beam-shell element model in Method II, and (*d*) the beam-shell element model in Method III
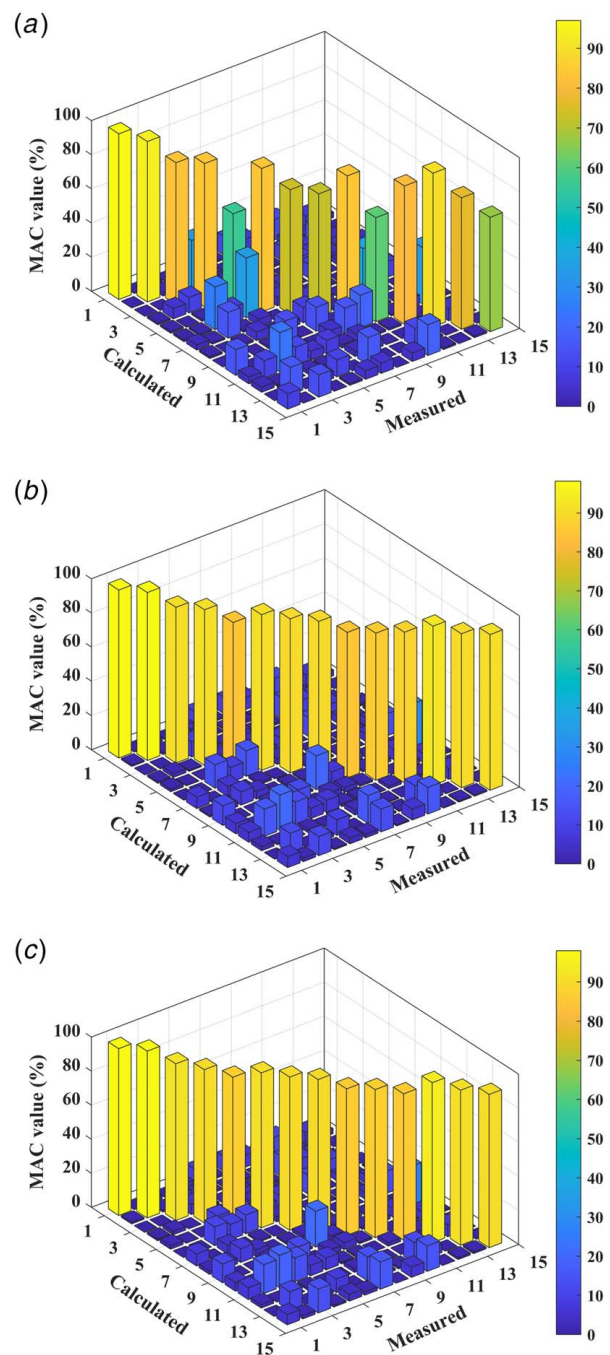

Fig. 30 MAC matrices between the first 14 elastic mode shapes of the specimen from the experiment and those from its beam-shell element models in Methods (*a*) I, (*b*) II, and (*c*) III

face sheets of the specimen was collected for 1 s and the associated resolution was 1 Hz.

4.2 Experimental Results. Experimental data of measurement points were collected by the Polytec Data Management System and analyzed by the LMS Test.Lab through use of the PolyMax algorithm. The sum of cross-power spectra between measurement points and the reference measurement point is shown in Fig. 26 to identify elastic modes of the specimen that exist in the selected frequency range of 1200–3200 Hz; note that its rigid-body natural frequencies in the frequency range of less than 1200 Hz are not shown there. A total number of 14 peaks that correspond to the first 14 elastic natural frequencies of the specimen were measured in the experiment, as shown in Fig. 26. Note that the ratio of the largest measured rigid-body natural frequency of the specimen to its first

elastic natural frequency is 16.8%, which is within the allowed 10–20% range mentioned in Ref. [30] for simulating free boundary conditions of the specimen. The absolute value of the maximum error between the first 14 elastic natural frequencies from the experiment and those from the solid element model in Sec. 3 is 4.6%, which indicates that the solid element model provides good estimates of elastic natural frequencies of the specimen compared with its experimental results.

The first 14 elastic natural frequencies of the specimen from the experiment are also compared with those from its beam-shell element models in Methods I, II, and III, as shown in Fig. 27. Errors between elastic natural frequencies from the experiment and beam-shell element models can be calculated by Eq. (13),

where f_i^{Solid} is replaced by f_i^{Measure}, which denotes the ith elastic natural frequency of the specimen from the experiment. Absolute values of maximum errors between the first 14 elastic natural frequencies from the experiment and those from beam-shell element models in Methods I, II, and III are 27.2%, 4.7%, and 4.1%, respectively, which occur for the fifth elastic mode in all the three methods. This indicates that ignoring welded joints in the beam-shell element model of the specimen in Method I significantly underestimates its elastic natural frequencies, and considering them in Methods II and III can provide their much better estimates.

Based on vibration data measured in the experiment, mode shapes of the specimen are obtained, and the first two and 14th elastic mode shapes are shown in Figs. 28 and 29(*a*), respectively, where dashed lines and rectangular marks denote undeformed positions of measurement points, and solid lines and circular marks denote their deformed positions. One can see from Fig. 28 that the first two elastic mode shapes of the specimen from the experiment are global torsional and bending modes, respectively, showing good agreement with results from its FE models in Figs. 20 and 21. The 14th elastic mode shape of the specimen from the experiment is selected to represent its high localized modes and compared with those from its beam-shell element models, as shown in Fig. 29. It can be seen from Fig. 29 that the 14th mode shape of the specimen from the experiment is a localized mode in edge areas of its face sheets, which is consistent with results from its beam-shell element models.

In order to quantitatively check correlation between the first 14 elastic mode shapes of the specimen from the experiment and those from its beam-shell element models in Methods I, II, and III, MAC matrices between them were calculated by Eq. (14), where ψ_i^{Solid} is replaced by ψ_i^{Measure}, which denotes the ith components of a mode shape vector of the specimen from the experiment, as shown in Fig. 30. By using Method I, diagonal MAC values are over 95% for the first two global elastic modes; they are less than 80% for most localized elastic modes, and less than 60% for some localized elastic modes, such as the fifth and tenth modes. By using Methods II and III, however, diagonal MAC values are over 95% for the first two global elastic modes and over 85% for the third through 14th localized elastic modes, which indicates that the first 14 elastic modes of the specimen were captured in the experiment without missing any modes and they have good correlation with those from its beam-shell element models in Methods II and III. Note that some off-diagonal MAC values in Figs. 30(*b*) and 30(*c*) are larger than 10% because use of only 50 measurement points in the experiment may not fully capture differences between mode shapes from the experiment and beam-shell element models in Methods II and III. Therefore, Methods II and III that consider welded joints in modeling of the PTSP are experimentally validated through above comparison between elastic natural frequencies and MAC matrices from the experiment and beam-shell element models in Methods II and III.

Errors between elastic natural frequencies and mode shapes of the specimen from the experiment and those from its solid element model and beam-shell element models in Methods II and III possibly arise from its geometrical discrepancies induced by the manufacturing process. As previously mentioned, FE models in this work are assumed to have ideal geometry, especially for welded joints. The actual PTSP specimen, however, may be fabricated with some defects, such as nonuniformity of welded joints and dislocation and nonparallelism of the two face sheets.

5 Conclusions

Two novel methods that consider welded joints in the PTSP as equivalent stiffnesses of beam and shell elements are developed to create its beam-shell element models, which can significantly simplify its solid element model. In these methods, equivalent stiffnesses are calculated by matching rotational displacements of a welded joint created by beam-shell element models with that created by the solid element model. The equivalent stiffness of beam elements is simulated by adding extra beam elements with corresponding cross-sectional dimensions, and that of shell elements is simulated by updating their Young's modulus in one method and their thickness in the other method. Elastic natural frequencies and mode shapes of beam-shell element models created by the proposed methods are compared with those from the solid element model and validated by operational modal analysis of a PTSP specimen. Main conclusions from this work are shown below:

(1) The equivalent stiffness of beam-shell element models of the PTSP in the two proposed methods can be determined by creating only the solid element model of a welded joint. Since no experiment is required to update equivalent stiffnesses of beam and shell elements in the two proposed methods, the methodologies developed here can be considered as predictive ones;

(2) Compared with the first 20 elastic natural frequencies from the solid element model of the PTSP, those from its directly simplified beam-shell element model that ignores welded joints are underestimated by 15–25%, while those from its beam-shell element models in the proposed methods are accurately determined and absolute values of errors are less than 2%, indicating that modeling of welded joints plays an important role in estimating natural frequencies of the PTSP;

(3) The first two elastic modes of the PTSP in this work are global modes, while the third through 20th modes are localized modes in edge areas of its face sheets and have different shapes for the two face sheets. MAC values between mode shapes from the beam-shell element model by updating the Young's modulus of shell elements and those from the solid element model are all over 95% along the diagonal of the MAC matrix and close to 0 for off-diagonal elements of the matrix, while MAC values between mode shapes from the beam-shell element model by updating the thickness of shell elements and those from the solid element model are less than 70% along the diagonal of the MAC matrix for some high localized modes, indicating that the method by updating the thickness of shell elements is less accurate in simulating high localized mode shapes of the PTSP than that by updating the Young's modulus;

(4) Compared with DOFs of the solid element model, those of beam-shell element models that are created by the proposed methods are reduced by 98% for the whole PTSP and 99% for each welded joint, indicating that the proposed methods can save large amounts of computation time and computer memory from the solid element model in the FE analysis of the PTSP with welded joints; and

(5) The first 14 elastic modes of the PTSP specimen were captured in the experiment without missing any modes. Absolute values of errors between elastic natural frequencies of the specimen from beam-shell element models in the proposed methods and the experiment are less than 2% for the first two global modes and less than 5% for the third through 14th localized modes. Diagonal MAC values are over 95% for the two global modes and over 85% for the localized modes. Accuracy of the proposed methods in estimating the first 14 elastic natural frequencies and mode shapes of the specimen is experimentally validated.

Conflict of Interest

There are no conflicts of interest.

Data Availability Statement

The datasets generated and supporting the findings of this article are obtainable from the corresponding author upon reasonable request. The authors attest that all data for this study are included in the paper.

References

[1] Evans, A. G., Hutchinson, J. W., Fleck, N. A., Ashby, M. F., and Wadley, H. N. G., 2001, "The Topological Design of Multifunctional Cellular Metals," Prog. Mater. Sci., **46**(3–4), pp. 309–327.

[2] Wadley, H. N., Fleck, N. A., and Evans, A. G., 2003, "Fabrication and Structural Performance of Periodic Cellular Metal Sandwich Structures," Compos. Sci. Technol., **63**(16), pp. 2331–2343.

[3] Ma, Y., Yan, H., and Xie, G., 2020, "Flow and Thermal Performance of Sandwich Panels With Plate Fins or/and Pyramidal Lattice," Appl. Therm. Eng., **164**(1), p. 114468.

[4] Smardzewski, J., 2019, "Wooden Sandwich Panels With Prismatic Core-Energy Absorbing Capabilities," Compos. Struct., **230**(12), p. 111535.

[5] Queheillalt, D. T., Murty, Y., and Wadley, H. N., 2008, "Mechanical Properties of an Extruded Pyramidal Lattice Truss Sandwich Structure," Scr. Mater., **58**(1), pp. 76–79.

[6] Wang, Z., Luan, C., Liao, G., Yao, X., and Fu, J., 2019, "Mechanical and Self-Monitoring Behaviors of 3D Printing Smart Continuous Carbon Fiber-Thermoplastic Lattice Truss Sandwich Structure," Compos. Part B: Eng., **176**(11), p. 107215.

[7] Azzouz, L., Chen, Y., Zarrelli, M., Pearce, J. M., Mitchell, L., Ren, G., and Grasso, M., 2019, "Mechanical Properties of 3-D Printed Truss-Like Lattice Biopolymer Non-Stochastic Structures for Sandwich Panels With Natural Fibre Composite Skins," Compos. Struct., **213**(4), pp. 220–230.

[8] Feng, L. J., Xiong, J., Yang, L. H., Yu, G. C., Yang, W., and Wu, L. Z., 2017, "Shear and Bending Performance of New Type Enhanced Lattice Truss Structures," Int. J. Mech. Sci., **134**(12), pp. 589–598.

[9] Yang, W., Xiong, J., Feng, L. J., Pei, C., and Wu, L. Z., 2020, "Fabrication and Mechanical Properties of Three-Dimensional Enhanced Lattice Truss Sandwich Structures," J. Sandwich Struct. Mater., **22**(5), pp. 1594–1611.

[10] Yang, J., Xiong, J., Ma, L., Wang, B., Zhang, G., and Wu, L., 2013, "Vibration and Damping Characteristics of Hybrid Carbon Fiber Composite Pyramidal Truss Sandwich Panels With Viscoelastic Layers," Compos. Struct., **106**(12), pp. 570–580.

[11] Li, S., Yang, J. S., Wu, L. Z., Yu, G. C., and Feng, L. J., 2019, "Vibration Behavior of Metallic Sandwich Panels With Hourglass Truss Cores," Marine Struct., **63**(1), pp. 84–98.

[12] Lu, L., Song, H., Yuan, W., and Huang, C., 2017, "Baseline-Free Damage Identification of Metallic Sandwich Panels With Truss Core Based on Vibration Characteristics," Struct. Health. Monit., **16**(1), pp. 24–38.

[13] Yuan, W., Song, H., Lu, L., and Huang, C., 2016, "Effect of Local Damages on the Buckling Behaviour of Pyramidal Truss Core Sandwich Panels," Compos. Struct., **149**(8), pp. 271–278.

[14] Syam, W. P., Wu, J., Zhao, B., Maskery, I., Elmadih, W., and Leach, R., 2018, "Design and Analysis of Strut-Based Lattice Structures for Vibration Isolation," Precis. Eng., **52**(4), pp. 494–506.

[15] Yang, J. S., Ma, L., Chaves-Vargas, M., Huang, T. X., Schröder, K. U., Schmidt, R., and Wu, L. Z., 2017, "Influence of Manufacturing Defects on Modal Properties of Composite Pyramidal Truss-Like Core Sandwich Cylindrical Panels," Compos. Sci. Technol., **147**(7), pp. 89–99.

[16] Radaj, D., Sonsino, C. M., and Fricke, W., 2006, *Fatigue Assessment of Welded Joints by Local Approaches*, 2nd ed., Woodhead Publishing, Cambridge, UK.

[17] Wang, Y. J., Zhang, Z. J., Xue, X. M., and Zhang, L., 2019, "Free Vibration Analysis of Composite Sandwich Panels With Hierarchical Honeycomb Sandwich Core," Thin-Walled Struct., **145**(12), p. 106425.

[18] Zhang, Z. J., Zhang, Q. C., Li, F. C., Yang, J. W., Liu, Z. Y., and Jin, F., 2019, "Modal Characteristics of Micro-Perforated Sandwich Beams With Square Honeycomb-Corrugation Hybrid Cores: A Mixed Experimental-Numerical Study," Thin-Walled Struct., **137**(4), pp. 185–196.

[19] Burlayenko, V. N., and Sadowski, T., 2009, "Analysis of Structural Performance of Sandwich Plates With Foam-Filled Aluminum Hexagonal Honeycomb Core," Comput. Mater. Sci., **45**(3), pp. 658–662.

[20] Yin, S., Chen, H., Wu, Y., Li, Y., and Xu, J., 2018, "Introducing Composite Lattice Core Sandwich Structure as an Alternative Proposal for Engine Hood," Compos. Struct., **201**(10), pp. 131–140.

[21] Qi, G., Ma, L., and Wang, S. Y., 2019, "Modeling and Reliability of Insert in Composite Pyramidal Lattice Truss Core Sandwich Panels," Compos. Struct., **221**(8), p. 110888.

[22] Zhou, J., and Li, Z., 2019, "Damage Detection Based on Vibration for Composite Sandwich Panels With Truss Core," Compos. Struct., **229**(12), p. 111376.

[23] Xu, S., and Deng, X., 2004, "An Evaluation of Simplified Finite Element Models for Spot-Welded Joints," Finite Elements Analysis Des., **40**(9–10), pp. 1175–1194.

[24] ABAQUS, 2011, *ABAQUS Standard User's Manuals*, Version 6.11, Hibbitt, Karlsson and Sorensen, Inc., Pawtucket, RI.

[25] Brown, A. M., and Seugling, R. M., 2004, "Using Plate Finite Elements for Modeling Fillets in Global Response Analysis," Finite Elem. Anal. Des., **40**(13–14), pp. 1963–1975.

[26] He, K., and Zhu, W. D., 2009, "Modeling of Fillets in Thin-Walled Beams Using Shell/Plate and Beam Finite Elements," ASME J. Vib. Acoust., **131**(5), p. 051002.

[27] He, K., and Zhu, W. D., 2011, "Finite Element Modeling of Structures With L-Shaped Beams and Bolted Joints," ASME J. Vib. Acoust., **133**(1), p. 011011.

[28] Kim, J. S., Xu, Y. F., and Zhu, W. D., 2020, "Linear Finite Element Modeling of Joined Structures With Riveted Connections," ASME J. Vib. Acoust., **142**(2), p. 021008.

[29] Deshpande, V. S., and Fleck, N. A., 2001, "Collapse of Truss Core Sandwich Beams in 3-Point Bending," Int. J. Solids Struct., **38**(36–37), pp. 6275–6305.

[30] Ewins, D. J., 2000, *Modal Testing: Theory, Practice, and Application*, 2nd ed., Research Studies Press Ltd., Baldock, Hertfordshire, UK.